

Linear Instability Analysis of the jetting regime for Co-flowing immiscible liquids in co-axial microtubes

In-Hwan Yang^{1,2+} and Mohamed S. El-Genk^{1,2,3,*}

¹Institute for Space & Nuclear Power Studies,

²Chemical & Nuclear Engineering Dept. and ³Mechanical Engineering Dept.
University of New Mexico, Albuquerque, NM, USA

Abstract

This paper applies the linear instability analysis to the prediction of the boundary between transition and jetting regimes for forming disperse droplets using co-flowing immiscible liquid in coaxial microtubes. Results are compared to a flow regimes map developed based on numerical simulations covering wide range of parameters and liquids properties. The results are also compared to reported experimental measurements for co-flowing ionized water and PDMS oil in coaxial microtubes. Although captures the general trend, the linear instability analysis consistently under predicts and over predict the boundary between transition and jetting at low and high Ca_d , respectively. This is because the analysis neglects the secondary perturbations and the inertia of the disperse liquid. Nonetheless, the linear instability analysis is a nearly accurate predicative approach that is much faster than performing Computation Fluid Dynamic (CFD) simulations or conducting experiments.

1. INTRODUCTION

There are three basic flow regimes for forming disperse droplets using co-flowing immiscible liquids in co-axial microtubes (Fig. 1 and Table 1), namely: dripping, transition (or poly-disperse dripping) and jetting. Shifting from one regime to the other occurs by changing the injection velocities and physical properties of the liquids, the interfacial tension and/or the diameters of the co-axial capillary tubes. Such changes also affect the size and formation frequency of the disperse droplets, and the common boundaries between the various regimes.

The dripping regime at low injection velocities produces monodisperse droplets. In this regime, pinching and an eventual breakup of the droplets occur at the exit of disperse liquid capillary nozzle by the interfacial tension force (Fig. 1a). When the diameter of the continuous liquid's microtube is much larger than that of the disperse liquid, forming disperse droplets are perfectly spherical and their radius decreases as the injection rate of the continuous liquid increases [1].

In the transition regime, at higher injection velocities than in the dripping regime, a short disperse-liquid thread forms, extending from the exit of the disperse liquid microtube to the growing droplet at the far end of the thread (Fig. 1b). Following a pinch-off of the droplet by interfacial tension, the liquid thread separates from the disperse liquid nozzle and becomes hydro-dynamically unstable, breaking off into a number of "satellite" droplets of miniature sizes (Fig. 1b). The average size of the primary droplet is typically smaller than in the dripping regime and depends on the injection velocities and physical properties of the co-flowing liquids. It also depends on the interfacial tension and the diameters of the coaxial microtubes [1,2,8]. Increasing the injection rate of the continuous liquid typically increases the length of disperse liquid thread, decreasing the size of the primary droplet, but increasing the number and sizes of the satellite droplets (Fig. 1b).

The shift to the jetting regime occurs by either increasing the injection velocities of the co-flowing immiscible liquids and/or decreasing the interfacial tension. These conditions increase the length of the

*Corresponding author: Regents' Professor and Director, Tel: (505) 277 - 5442, E-mail: mgenk@unm.edu

+Current affiliation: School of Mechanical Engineering, Korea University, Seoul, Korea

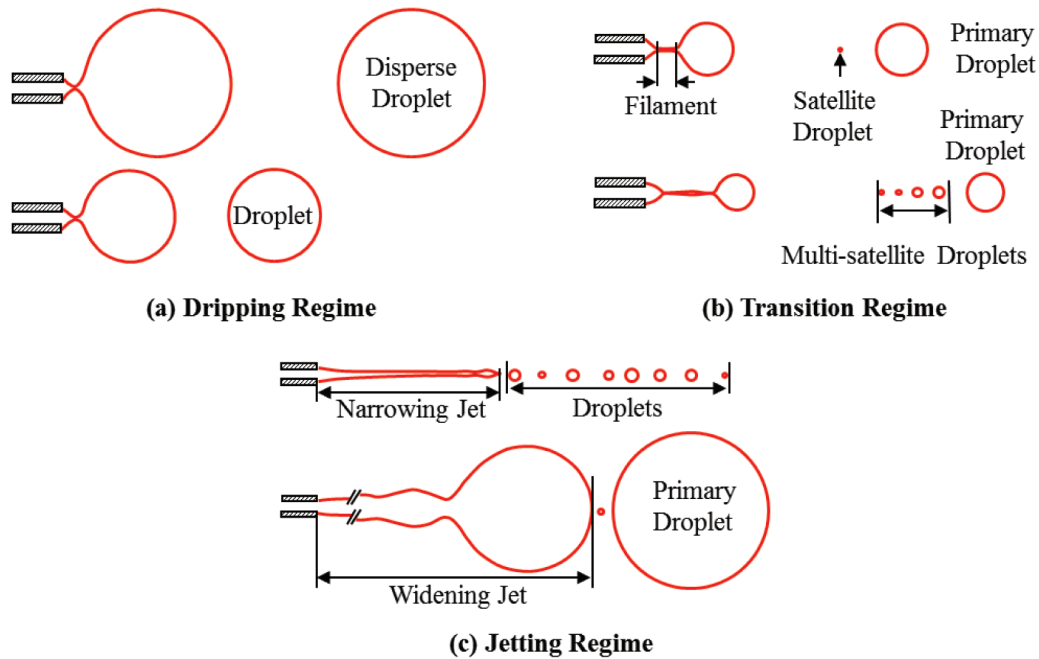


Figure 1. Regimes for forming disperse droplets for co-flowing immiscible liquids [8].

disperse-liquid thread, which eventually evolves into either a stable narrowing or widening jet (Fig. 1c). Disperse droplets form and break off at the tip of these jets by the combined effect of viscous forces of the co-flowing liquids, interfacial tension, and hydrodynamic instability [2-8,19,23].

More than a century ago, Rayleigh [9,10] conducted a linear instability analysis of a liquid jet in air. The analysis assumed that an initially unperturbed surface of an infinitely long liquid jet could become unstable due to the growth of linear perturbations along the surface with time, eventually causing a breakup of the jet. In his analysis [9,10], the axisymmetrically perturbed interface had an amplifying sinusoidal wave, $\xi = \xi_0 e^{i(kz - \omega t)}$ with a small initial amplitude (ξ_0). Tomotika [11] extended Rayleigh's instability analysis to co-flowing immiscible liquids by accounting for the effect of the continuous liquid viscosity. The work of Rayleigh and Tomotika [9-11] has been the foundation of recent development and application of linear instability analysis to co-flowing immiscible liquids in coaxial microtubes.

This hydrodynamic instability analysis applies to the conditions for the jetting regime of forming disperse droplets. The analysis accounts for the spatial and temporal growth of the amplitude of a surface perturbation [5,6,12-19]. The amplitude increases exponentially, not only with time, but also with axial location along the interface separating the flows of the disperse and continuous liquids. Depending on the spatial and temporal growth of the amplitude, the breakup of a disperse droplet from a stable disperse liquid jet could be caused by either an absolute or a convective instability. In the absolute instability, interface disturbances grow and propagate upstream, eventually pinching off the disperse droplet close to the exit of the inner microtube (Figs. 1a and 1b). On the other hand, the breakup of disperse droplets at the far end of a stable liquid jet is caused by the convective instability (Fig. 1c). The preferential downstream propagation of growing surface perturbations in the convective instability eventually pinches off the disperse droplet at the tip of a long disperse-liquid jet (Fig. 1c).

Guillot et al. [5], Guillot, Colin, and Ajdari [19], and Herrada, G.-Calvo, and Guillot [6], assuming creep flows, analytically derived the dispersion relation between the complex frequency and the wave number. Thus, the inertial forces of the co-flowing liquids are negligibly small compared to their viscous forces. In their linear instability analysis, Guillot et al. [5] radially averaged the flow and the perturbation of the co-flowing liquids and neglected their inertia. They also performed experiments, employing disperse aqueous solution of 50 wt% glycerin and silicon oil as the continuous liquid. These liquids have viscosities of 55 mPa.s and 235 mPa.s, respectively. The radii of the co-axial capillaries for injecting the continuous and disperse liquids varied from 200-500 μm and 20-50 μm , respectively. The trend of their instability analysis results generally agreed with the experimental measurements, when plotting the flow rate of the disperse liquid versus that of the continuous liquid. At low flow rates of the disperse liquid, the predicted flow rates of the continuous liquid at the boundary between the transition and jetting regimes were much higher than the experimental results.

Table 1. Disperse droplets regimes for co-flowing immiscible liquids [8].

Item	Flow Regime			
	Dripping	Transition	Jetting	
			Narrow	Wide
Condition	Moderate velocities, high interfacial tension, low viscous drag	Higher velocities and lower interfacial tension	High continuous liquid injection & interfacial tension	Low continuous liquid injection & interfacial tension
Emulsion	Mono-disperse droplets	Mono-disperse primary droplets, followed by tiny satellite droplets	Poly-disperse droplets of small sizes	Mostly mono-disperse droplets with a few tiny satellite droplets
Primary droplets break off	Pinch-off by interfacial tension at exit of disperse liquid microtube	Pinch-off by interfacial tension at far end of thin short disperse liquid thread	Hydrodynamic instability at far end of stable disperse liquid jets	
Satellite disperse droplets	Rare, depending on conditions	By breakup of disperse liquid thread	Infrequent, following break off of primary droplets	
Formation frequency	Lower than transition & narrowing jet, but higher than widening jet	Higher than dripping & widening jet, but lower than narrowing jet	Very high	Very low
Primary droplet size	Larger than transition & narrowing jet but lower than widening jet	Much smaller than in dripping and wide jetting regimes	Smallest	Largest

Herrada et al. [6] have developed an axisymmetric instability model, similar to that of Guillot et al. [5], but accounted for the inertia of both the co-flowing liquids. They considered 3-D perturbed liquid flows

and compared the results of the instability analysis with their experimental measurements. They developed a regimes map in terms of the flow rates of the co-flowing liquids, similar to Guillot et al. [5]. Only at high flow rates of the disperse liquid, the predicted flow rates of the continuous liquid for the boundary between transition and jetting agreed with the experiments. The experiments of Herrada et al. [6] varied the diameter of the disperse liquid microtube from 40-100 μm and that of the continuous liquid flow was either 550 or 860 μm . Their experiments were conducted using three pairs of disperse and continuous liquids (water with a viscosity of 1.0 mPa.s and hexadecane with a viscosity of 3 mPa.s, water-glycerin solution with a viscosity of 55 mPa.s and silicone oil with a viscosity of 235 mPa.s, and water-glycerin solution with a viscosity 650 mPa.s and silicone with a viscosity of 235 mPa.s). They controlled the interfacial tension in the experiments by adding sodium dodecyl sulfate to the aqueous solutions and Span-80 to the hexadecane.

Utada et al. [3] and Castro-Hernandez et al. [4] have introduced a flow regimes map that characterizes the boundary between transition and jetting, assuming transition is a part of the dripping regime (Figs. 1a and 1b). These flow regimes map are based on the capillary number of the continuous liquid, Ca_c , and the Weber number of the disperse liquid, We_d . When the exerted viscous and inertial forces of the co-flowing immiscible liquids on the interface outweigh that of interfacial tension, a disperse-liquid jet forms. Narrowing jets (Fig. 1c) from when the viscous shear of the continuous liquid helps overcome the effect of the interfacial tension. On the other hand, widening jets from when increasing the viscous shear of the disperse liquid. The inertial force of the creeping disperse liquid flow is negligibly small ($Re_d < 1$).

Castro-Hernandez et al. [4] did not perform instability analysis, but conducted experiments to investigate the criteria of Utada et al. [3] for the predicting the boundary between transition and widening jetting. Their results indicated the shift from transition to jetting occurs at a lower Weber number of the disperse liquid, We_d , than reported by Utada et al. [3]. They also confirmed that only when Reynolds number of the disperse liquid, $Re_d > 1.0$, Weber number, We_d , can be used to indicate the shift to jetting [4].

Several assumptions have been made to simplify the complex mathematical formulations of the linear instability for predicting the conditions for the jetting regime. These include neglecting higher order perturbations of the interface and the radial component of the surface perturbations, and assuming creep flows and that the transition regime (Fig. 1b) is as a part of dripping (Fig. 1a). Although the reported analysis results provided valuable insights, they were inconclusive and there was not a unified criterion for accurately predicting the boundary between transition and jetting.

Recently, the authors [8] conducted extensive numerical simulations covering wide ranges of parameters, including the microtubes radii, the properties of the co-flowing liquids, and the interfacial surface tension. The numerical results were used to generate motion picture movies to accurately identify the prevailing regime and the conditions for shifting from dripping to transition and from transition to jetting. The results were also used to develop semi-empirical dimensionless correlations for predicting the boundaries between dripping, transition and jetting in terms the Capillary number of the disperse liquid (Ca_d), the dynamic force ratio of the continuous and disperse liquids ($\mu_r \bar{u}_r$), and the ratio of the microtubes radii (R^*). The correlations were in good agreements with the numerical simulation results and the reported experimental data for different immiscible liquids. These include ionized water and PDMS (Polydimethylsiloxane) oil with $R^* = 10$, and aqueous solutions of glycerine into silicone oil flow with and without surfactant (Sodium Dodecyl Sulfate) with $R^* = 13.8$ [3,5,6].

The objective of this work is to perform hydrodynamic linear instability analysis and compare the results to the recently developed dimensionless correlation by the authors [8] and the reported experimental results [3] for the boundary between transition and jetting. Presented and discussed next are the constituent equations, initial and boundary conditions, the solution methodology for the hydrodynamic linear instability and the dispersion relation that is identical to those of Herrada, G.-Calvo, and Guillot [6].

2. HYDRODYNAMIC INSTABILITY ANALYSIS

The instability analysis assumes an infinite cylindrical thread of the disperse liquid as “a basic flow” in a coaxial flowing continuous liquid and treats the perturbed interface using linear perturbation equation. Fig. 2 presents an illustration that compares unperturbed and perturbed interfaces of a disperse liquid jet

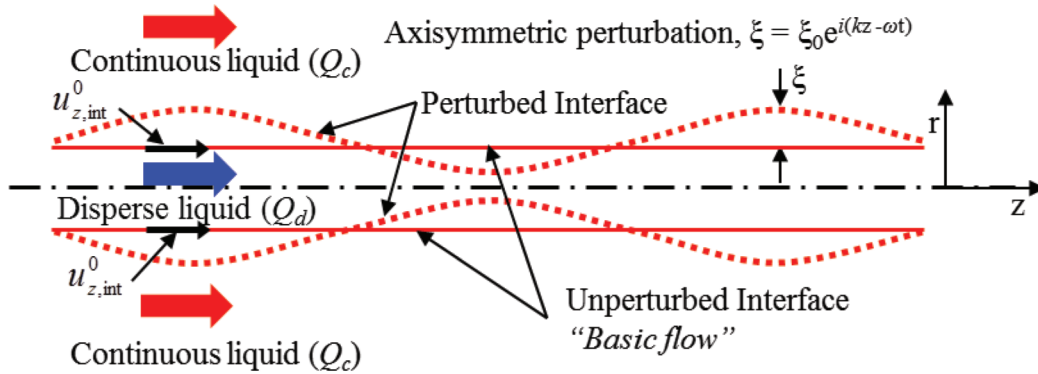


Figure 2. Growth of the perturbations propagating along the surface of disperse liquid jet in a co-flowing continuous liquid.

in a co-flowing immiscible liquid. The initial basic instability of the interface grows or decays, depending on the hydrodynamic drag and inertia forces of the co-flowing liquids and the value of the interfacial tension. The growth and decay of the perturbed interface is characterized by traveling linear waves. The present analysis examines the stability of the interface by solving the constituent equations and the dispersion relation. It predicts the conditions of forming a stable, disperse liquid jet and the breakup of disperse droplets from the jet. The perturbed velocity and pressure of the basic disperse liquid flow are expressed as:

$$u_n = u_n^0 + u'_n, \tag{1a}$$

$$p_n = p_n^0 + p'_n \tag{1b}$$

$$\kappa = \kappa' + \kappa^0 = \kappa' - \frac{1}{r_j^0} \tag{1c}$$

In these equations, u_n^0 and p_n^0 are the velocity and the pressure vectors of the basic flow, u'_n and p'_n are the vectors for the perturbations in the velocity and the pressure, respectively, and κ^0 and κ' are the basic curvature and the induced perturbation in the curvature of the interface between the co-flowing disperse and continuous liquids (Fig. 2). The interfacial tension is kept constant, which is not applicable to the case of added surfactant to the disperse liquid. The gradient of the surfactant along the interface would stimulate Marangoni convection, altering the results and complicating the linear instability analysis. For simplicity, the present analysis also neglects the effect of the secondary perturbation and the radial velocity components of the interface (Fig. 3). These assumptions, although simplify the problem for obtaining a closed form analytical solution, could affect the predictions of the boundary between transition and jetting. The perturbations along the surface of disperse liquid jet are characterized by a linear wave function.

The governing equations for implementing the hydrodynamic linear instability analysis are [8]:

(a) Continuity equation;

$$\frac{\partial \rho_n}{\partial t} + \rho_n \nabla \cdot \vec{v}_n = 0 \tag{2}$$

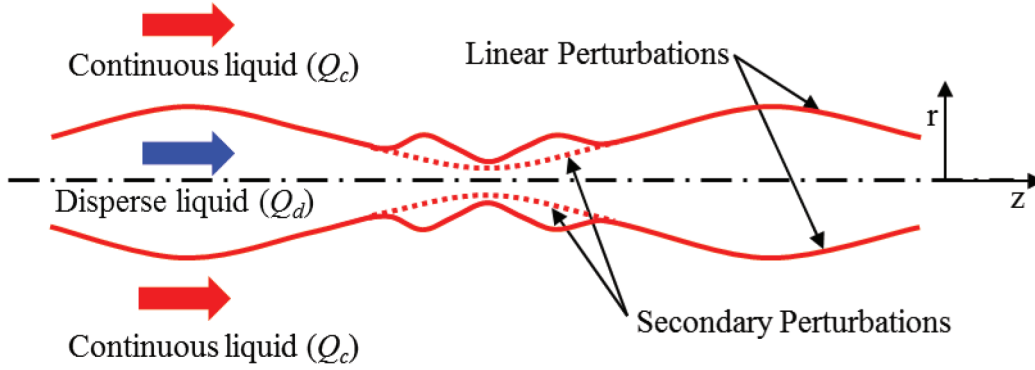


Figure 3. Growth of propagating linear and secondary perturbations along the surface of a disperse liquid jet in a co-flowing continuous liquid.

(b) Momentum balance equations:

$$\rho_n \frac{\partial u'_n}{\partial t} + \rho_n (u'_n \cdot \nabla u_n^0 + u_n^0 \cdot \nabla u'_n + u'_n \cdot \nabla u'_n) = -\nabla p' + \mu_n \nabla^2 u'_n + \rho_n g \quad (3)$$

The initial interface of the basic disperse liquid flow grows or decays, depending on the values of the hydrodynamic drag and inertial forces induced by the co-flowing liquids and the interface tension force. The radial location of the interface in the flow domain, r_j , and the perturbed velocities and pressures of the continuous and disperse liquids are expressed in cylindrical coordinates (r, z) as:

$$\begin{aligned} r_j(z, t) &= r_j^0 + \xi e^{i(kz - \omega t)} \\ u'_n(r, z, t) &= \hat{u}_n(r) e^{i(kz - \omega t)} \\ p'_n(r, z, t) &= \hat{p}_n(r) e^{i(kz - \omega t)} \end{aligned} \quad (4)$$

In these equations, r_j^0 is the initial radial location of the interface of the basic disperse liquid flow, k is the wave number, ω is the frequency, and ξ is the initial amplitude of the perturbed interface ($\xi \ll 1$) (Fig. 2). After substituting equation (4) into equations (2) and (3), the resulting equations are linearized by neglecting the squares and dot products of the perturbed velocity components as well as the gravity force. The obtained momentum balance and continuity equations of the disperse and continuous co-flowing liquids are expressed, respectively, as:

(a) Momentum balance equations in the radial coordinate, r :

$$\begin{aligned} -\rho_n \omega \hat{u}_{r,n} + \rho_n k i u_{z,n}^0 \hat{u}_{r,n} \\ = -\frac{\partial \hat{p}_n}{\partial r} + \mu_n \left(\frac{1}{r} \frac{\partial}{\partial r} \left(r \frac{\partial \hat{u}_{r,n}}{\partial r} \right) - k^2 \hat{u}_{r,n} - \frac{\hat{u}_{r,n}}{r^2} \right) \end{aligned} \quad (5a)$$

(b) Momentum balance equations in the axial coordinate, z :

$$\begin{aligned} -p_n \omega \hat{u}_{z,n} + \rho_n k i u_{z,n}^0 \hat{u}_{z,n} + \rho_n \hat{u}_{r,n} \frac{\partial u_{z,n}^0}{\partial r} \\ = -ik \hat{p}_n + \mu_n \left(\frac{1}{r} \frac{\partial}{\partial r} \left(r \frac{\partial \hat{u}_{z,n}}{\partial r} \right) - k^2 \hat{u}_{z,n} \right) \end{aligned} \quad (5b)$$

(c) Continuity equations:

$$ik \hat{u}_{z,n} + \frac{1}{r} \frac{\partial (r \hat{u}_{r,n})}{\partial r} = 0 \quad (6)$$

Applying the creeping flow approximation omits the inertial terms on the left hand side of the momentum balance equations (5a and 5b). Thus, the resulting simplified equations, expressed in a dimensionless form, are given as:

$$-\frac{\partial \hat{p}_n^*}{\partial r^*} + \frac{\mu_n^*}{\text{Re}_{\text{int}}} \left(\frac{1}{r^*} \frac{\partial}{\partial r^*} \left(r^* \frac{\partial \hat{u}_{r,n}^*}{\partial r^*} \right) - k^{*2} \hat{u}_{z,n}^* - \frac{\hat{u}_{r,n}^*}{r^{*2}} \right) = 0 \quad (7a)$$

$$-ik^* \hat{p}_n^* + \frac{\mu_n^*}{\text{Re}_{\text{int}}} \left(\frac{1}{r^*} \frac{\partial}{\partial r^*} \left(r^* \frac{\partial \hat{u}_{z,n}^*}{\partial r^*} \right) - k^{*2} \hat{u}_{z,n}^* \right) = 0 \quad (7b)$$

Similarly, equation (6) is expressed as:

$$ik^* \hat{u}_{z,n}^* + \frac{1}{r^*} \frac{\partial (r^* \hat{u}_{r,n}^*)}{\partial r^*} = 0 \quad (8)$$

Equation (4), expressed in dimensionless form, is given as:

$$\begin{aligned} r_j^*(z, t) &= 1 + \xi e^{i(k^* z^* - \omega^* t^*)} \\ u_n^*(r, z, t) &= \hat{u}_n^*(r) e^{i(k^* z^* - \omega^* t^*)} \end{aligned} \quad (9)$$

The axial and radial perturbation velocities are expressed in terms of the stream-function, ψ , as:

$$\hat{u}_{z,n}^* = \frac{1}{r^*} \frac{\partial}{\partial r^*} (r^{*2} \psi_n^*), \quad (10a)$$

and,

$$\hat{u}_{r,n}^* = -ik^* r^* \psi_n^* \quad (10b)$$

Substituting these equations, which satisfy the continuity equations (8), and eliminating the perturbed pressure, the stream-functions for the perturbed flows for the stream-functions of the disperse and continuous liquids can be expressed as:

(a) Disperse liquid:

$$\psi_d = \frac{1}{r^*} \{ C_1 I_1(k^* r^*) + C_1 I_3(k^* r^*) + C_2 K_1(k^* r^*) + C_2 K_3(k^* r^*) \} + C_7 I_0(k^* r^*) + C_8 K_0(k^* r^*) \quad (11a)$$

(b) Continuous liquid:

$$\psi_c = \frac{1}{r^*} \{ C_3 I_1(k^* r^*) + C_3 I_3(k^* r^*) + C_4 K_1(k^* r^*) + C_4 K_3(k^* r^*) \} + C_5 I_0(k^* r^*) + C_6 K_0(k^* r^*) \quad (11b)$$

In these equations, $C_1 - C_8$ are arbitrary constants. The perturbed radial velocity and the gradient of the axial perturbed velocity of the disperse liquid along the centerline of the flow domain ($r^* = 0$), are zero due to symmetric condition (i.e. $\hat{u}_{r,d}^*|_{r^*=0} = 0$, and $\partial \hat{u}_{z,d}^* / \partial r^* = 0$). Therefore, the modified Bessel functions of the second kind terms, $K_0(k^* r^*)$, $K_1(k^* r^*)$, and $K_3(k^* r^*)$, in the stream-function expression for the disperse liquid (equation (11a)) drop out. In addition, the third order, modified Bessel functions of the first and second kind, $I_3(k^* r^*)$, and $K_3(k^* r^*)$, for both co-flowing liquids are negligible [6], thus eliminated from equations (11a) and (11b). Thus, the resulting stream-function equations for the continuous and disperse liquids are expressed as:

(a) Disperse liquid:

$$\psi_d = \frac{1}{r^*} C_1 I_1(k^* r^*) + C_2 I_0(k^* r^*) \quad (12a)$$

(b) Continuous liquid:

$$\psi_c = \frac{1}{r^*} \{ C_3 I_1(k^* r^*) + C_4 k_1(k^* r^*) \} + C_5 I_0(k^* r^*) + C_6 I_0(k^* r^*) \quad (12b)$$

In order to determine the six coefficients in these two equations, six additional equations are needed, which obtained from applying the following: (a) non-slip condition at the walls, (b) continuity of the flow field at the interface, and (c) the momentum jump condition at the interface. The radial velocity of the continuous flow at the wall of the outer microtube is zero, $\hat{u}_{r,c}^*|_{r^*=R_c^*} = 0$ and with no-slip at the wall, $\hat{u}_{z,c}^*|_{r^*=R_c^*} = 0$. Applying these boundary conditions to equation (12b) gives:

$$C_3 k^* I_0(k^* R_c^*) + C_5 (2I_0(k^* R_c^*) + k^* R_c^* I_1(k^* R_c^*)) - C_4 k^* K_0(k^* R_c^*) + C_6 (2K_0(k^* R_c^*) - k^* R_c^* K_1(k^* R_c^*)) = 0 \quad (13a)$$

and,

$$\begin{aligned}
 & -C_5 ik^* R_c^* I_0(k^* R_c^*) - C_3 ik^* I_1(k^* R_c^*) \\
 & -C_6 ik^* R_c^* K_0(k^* R_c^*) - C_4 k^* K_1(k^* R_c^*) = 0
 \end{aligned} \tag{13b}$$

At the interface between the two co-flowing liquids ($r^* = 1$) the perturbed velocities of the disperse and continuous liquids are equal (i.e., $\hat{u}_{r,d}^* = \hat{u}_{r,c}^*$ and $\hat{u}_{z,d}^* = \hat{u}_{z,c}^*$). Substituting these conditions, together with equations (12a) and (12b) into equations (10a) and (10b), gives:

$$\begin{aligned}
 & -C_1 ik^* I_1(k^*) + C_3 ik^* I_1(k^*) + C_4 ik^* K_1(k^*) \\
 & -C_2 ik^* I_0(k^*) + C_5 ik^* I_0(k^*) + C_6 ik^* K_1(k^*) = 0
 \end{aligned} \tag{14a}$$

and,

$$\begin{aligned}
 & C_1 k^* I_0(k^*) - C_3 k^* I_0(k^*) + C_4 k^* K_0(k^*) + C_2 (2I_0(k^*) + k^* I_1(k^*)) \\
 & + C_5 (-2I_0(k^*) - k^* I_1(k^*)) + C_6 (-2K_0(k^*) + k^* K_1(k^*)) = 0
 \end{aligned} \tag{14b}$$

The final two equations are obtained from satisfying the dynamic force balance (or momentum jump condition) at the interface [1,8], with the introduced perturbation of the interface (equation (3)). Thus, the shear tensor (τ'_n) for the continuous and disperse liquids can be expressed as:

$$\tau'_n = \begin{bmatrix} -P'_{r,n} + \tau'_{rr,n} & \tau'_{rz,n} \\ \tau'_{zr,n} & -P'_{z,n} + \tau'_{zz,n} \end{bmatrix} \tag{15}$$

Both the axial and radial components of the interfacial shear stress generally affect the movement of the interface and the perturbation of the interface is caused by both the axial and radial components of the liquid motion. In the linear stability analysis, however, the perturbed interface is treated as a plane wave whereas the perturbing motion of the interface is the results of the momentum transfer only in the radial direction ($\tau'_{rz,n} = 0$ and $\tau'_{zr,n} = 0$). Thus, considering the radial components of the interfacial shear forces, equation (15) becomes:

$$\tau'_n = \begin{bmatrix} -P'_{r,n} + 2\mu_n \frac{\partial u'_{r,n}}{\partial r} & 0 \\ \mu_n \left(\frac{\partial u'_{r,n}}{\partial z} + \frac{\partial u'_{z,n}}{\partial r} \right) & 0 \end{bmatrix} \tag{16}$$

The force balance at the interface is expressed as:

$$\left(-P'_c + 2\mu_c \frac{\partial u'_{r,c}}{\partial r}\right) - \left(-P'_d + 2\mu_d \frac{\partial u'_{r,d}}{\partial r}\right) = \sigma_{d,c} \left(\kappa' - \frac{1}{r_j^0}\right) \quad (17a)$$

And the axial component of the interfacial shear stress is given as:

$$\mu_c \left(\frac{\partial u'_{r,c}}{\partial z} + \frac{\partial u'_{z,c}}{\partial r}\right) - \mu_d \left(\frac{\partial u'_{r,d}}{\partial z} + \frac{\partial u'_{z,d}}{\partial r}\right) = 0 \quad (17b)$$

Substituting equations (4) into (17a) and (17b) and rearranging the results, give the following equations for the radial and axial components of the interfacial shear stress:

(a) Radial component of the interfacial shear stress:

$$\left(-\hat{P}_c + 2\mu_c \frac{\partial \hat{u}_{r,c}}{\partial r}\right) - \left(-\hat{P}_d + 2\mu_d \frac{\partial \hat{u}_{r,d}}{\partial r}\right) = -\sigma_{d,c} \left(\frac{\xi}{r_j^{0^2}}\right) (1 - k^2 r_j^{0^2}) \quad (18a)$$

(b) Axial component of the interfacial shear stress

$$\mu_c \left(ik \hat{u}_{r,c} + \frac{\partial \hat{u}_{z,c}}{\partial r}\right) - \mu_d \left(ik \hat{u}_{r,d} + \frac{\partial \hat{u}_{z,d}}{\partial r}\right) = 0 \quad (18b)$$

These equations expressed in dimensionless form are:

$$\left(-Re_{int} \hat{P}_c^* + 2\mu_r \frac{\partial \hat{u}_{r,c}^*}{\partial r^*}\right) - \left(-Re_{int} \hat{P}_d^* + 2\mu_r \frac{\partial \hat{u}_{r,d}^*}{\partial r^*}\right) = -(\xi^* (1 - k^{*2}) / Ka), \quad (19a)$$

and,

$$\mu_r \left(ik^* \hat{u}_{r,c}^* + \frac{\partial \hat{u}_{z,c}^*}{\partial r^*}\right) - \mu_r \left(ik^* \hat{u}_{r,d}^* + \frac{\partial \hat{u}_{z,d}^*}{\partial r^*}\right) = 0 \quad (19b)$$

The kinematic boundary condition is used to find the dimensionless amplitude of the perturbed interface (ξ^*) in equation (19a). This condition states that the radial and axial velocity components of disperse and continuous co-flowing liquids at the interface equal those of the interface itself. Thus, at any radial location, $r_j(z, t)$, the interface moves with the same velocity as the disperse liquid. The radial location, and hence the amplitude, ξ^* , of the interface perturbation is obtained from the solution of following equation [20,21]:

$$\frac{\partial r_j}{\partial t} + u_d \Big|_{r=r_j^0} \cdot \nabla r_j = 0 \quad (20a)$$

This equation can also be written as:

$$\frac{\partial r_j}{\partial t} + u_{z,d} \Big|_{r=r_j^0} \frac{\partial r_j}{\partial z} - u_{r,d} \Big|_{r=r_j^0} = 0 \tag{20b}$$

Substituting for the total flow velocity in this equation from equation (4), neglecting the axial perturbed velocity, $u'_{z,d}$, and rearranging the result give the following equation:

$$-\xi i \omega + u_{z,d}^0 \Big|_{r=r_j^0} \xi i k - \hat{u}_{r,d} \Big|_{r=r_j^0} = 0, \tag{21a}$$

This equation expressed in a dimensionless form as:

$$-\xi^* i (\omega^* - k^*) + \hat{u}_{r,d}^* \Big|_{r=r_j^0} = 0. \tag{21b}$$

In this equation, the amplitude (ξ^*) is eliminated by substituting equation (21b) into (19a), which yields:

$$\left(-Re_{int} \hat{P}_c^* + 2\mu_r \frac{\partial \hat{u}_{r,c}^*}{\partial r^*} \right) - \left(-Re_{int} \hat{P}_d^* + 2 \frac{\partial \hat{u}_{r,d}^*}{\partial r^*} \right) = \frac{\hat{u}_{r,d}^* \Big|_{r^*=1}}{i(\omega^* - k^*)} \frac{1 - k^{*2}}{Ka} \tag{22}$$

The dimensionless pressure terms ($Re_{int} \hat{P}_c^*$ and $Re_{int} \hat{P}_d^*$) in this equation are obtained from the solution of equation (7b) together with equations (9a) and (9b). Equations (22) and (19b) are rewritten by expressing the velocities of the continuous and disperse liquids in terms of the stream function (equations (10a), (10b), (13a), and (13b)). The resulting equations are given, as:

$$\begin{aligned} & C_1 \left(2ik^{*2} I_0(k^*) - 2ik^* I_1(k^*) + \frac{k^*(k^{*2} - 1) I_1(k^*)}{Ka(k^* - \omega^*)} \right) - 2iC_5 k^{*2} \mu_r I_1(k^*) + \\ & C_3 (2ik^* \mu_r I_1(k^*) - 2ik^{*2} \mu_r I_0(k^*)) + 2iC_6 k^{*2} \mu_r K_1(k^*) + \\ & C_4 (2ik^* \mu_r K_1(k^*) + 2ik^{*2} \mu_r K_0(k^*)) + \\ & C_2 \left(\left(\frac{k^*(k^{*2} - 1) I_0(k^*)}{Ka(k^* - \omega^*)} \right) \right) + 2ik^{*2} I_1(k^*) = 0 \end{aligned} \tag{23a}$$

and,

$$\begin{aligned} & 2iC_1 k^* I_1(k^*) - 2iC_3 k^{*2} \mu_r I_1(k^*) + C_2 (2k^{*2} I_0(k^*) + 2k^* I_1(k^*)) \\ & + C_5 (-2k^{*2} \mu_r I_0(k^*) + 2k^* \mu_r I_1(k^*)) - 2C_4 k^{*2} \mu_r K_1(k^*) \\ & + C_6 (-2k^{*2} \mu_r K_0(k^*) + 2k^* \mu_r K_1(k^*)) = 0 \end{aligned} \tag{23b}$$

In equation (23a), Ka is the capillary number of the disperse liquid at the interface of the basic flow. The six equations (13, 14, and 23) constitute a homogeneous linear system that involves six unknown

constants (C_1 to C_6). The amplitude of the perturbations at the interface equals the eigenvalues calculated using equation (24). Note that the determinant of the square matrix on the left-hand side of equation (24) should be zero.

$$\begin{pmatrix} 2k^{*2}I_1(k^*) & A_2 & -2k^{*2}\mu_r I_1(k^*) & -2k^{*2}\mu_r K_1(k^*) & A_5 & A_6 \\ B_1 & B_2 & B_3 & B_4 & -2ik^{*2}\mu_r I_1(k^*) & 2ik^{*2}\mu_r K_1(k^*) \\ -ik^* I_1(k^*) & -ik^* I_0(k^*) & ik^* I_1(k^*) & ik^* K_1(k^*) & ik^* I_0(k^*) & ik^* K_0(k^*) \\ k^* I_0(k^*) & D_2 & -k^* I_0(k^*) & k^* K_0(k^*) & D_5 & D_6 \\ 0 & 0 & k^* I_0(k^* R_c^*) & -k^* K_0(k^* R_c^*) & E_5 & E_6 \\ 0 & 0 & -ik^* I_1(k^* R_c^*) & -ik^* K_1(k^* R_c^*) & -ik^* R_c^* I_1(k^* R_c^*) & -ik^* R_c^* K_0(k^* R_c^*) \end{pmatrix} \begin{pmatrix} C_1 \\ C_2 \\ C_3 \\ C_4 \\ C_5 \\ C_6 \end{pmatrix} = 0 \quad (24)$$

The constants $A_2, A_5, A_6, B_1, B_2, B_3, B_4, D_2, D_5, D_6, E_5,$ and E_6 are expressed as:

$$\begin{aligned} A_2 &= 2k^{*2}I_0(k^*) + 2k^* I_1(k^*), \quad A_5 = -2k^{*2}\mu_r I_0(k^*) - 2k^* \mu_r I_1(k^*), \\ A_6 &= -2k^{*2}\mu_r K_0(k^*) + 2k^* \mu_r K_1(k^*), \\ B_1 &= 2ik^{*2}I_0(k^*) - 2ik^* I_1(k^*) + (k^*(k^{*2} - 1)I_1(k^*)/Ka(k^* - \omega^*)), \\ B_2 &= (k^*(k^{*2} - 1)I_0(k^*)/ka(k^* - \omega^*)) + 2ik^{*2}I_1(k^*), \\ B_3 &= 2li^{*2}\mu_r I_0(k^*) + 2ik^* \mu_r I_1(k^*) \quad B_4 = 2ik^{*2}I_1 \mu_r K_0(k^*) + 2ik^{*2}\mu_r K_0(k^*), \\ D_2 &= 2I_0(k^*) + k^* I_1(k^*), \quad D_5 = -2I_0(k^*) - k^* I_1(k^*), \\ D_6 &= -2K_0(k^*) + k^* K_1(k^*), \quad E_5 = 2I_0(k^* R_c^*) + k^* R_c^* I_1(k^* R_c^*), \\ E_6 &= 2K_0(k^* R_c^*) - k^* R_c^* K_1(k^* R_c^*). \end{aligned} \quad (25)$$

The square matrix in equation (24) is a very long equation in terms of $k^*, \omega^*, Ka, R_c^*,$ and μ_r . The rearranged equation gives the following expression for the dimensionless wave frequency, as:

$$\omega^* = k^* - i(k^*(k^{*2} - 1)NM / (2KaDn)) \quad (26)$$

In this equation, the functions NM and Dn are expressed in terms of k^*, R_c^* and μ_r by equations (A.1) and (A.2) in Appendix-A. Equation (26) determines the values for the absolute and convective instabilities corresponding to the transition and jetting regimes, respectively. In the present linear instability analysis, both the wave number and frequency are complex numbers, so that the growth of the amplitude of the surface perturbations depend exponentially on $(\omega^* - k^*)$. The values of both $IM[\omega^*]$ and $IM[-k^*]$ should be positive for the interface to become unstable due to the temporal and spatial growths of the amplitude of the interface perturbations. These perturbations travel at a velocity, $IM[\omega^*]/IM[-k^*]$.

A droplet breakup from the tip of a stable disperse liquid jet is affected by the traveling perturbation velocity of the interface. Thus, the position where a stable liquid jet breaks up can be predicted by the value of the traveling perturbation velocity at the interface. When this velocity is positive, the growing perturbations of the interface propagate downstream (convective instability), and when the velocity is negative, the growing surface perturbations propagate upstream toward the exit of disperse liquid microtube (absolute instability). Thus, the breakup of a disperse droplet in the jetting regime, the result of convective instability occurs when the spatial growth rate of the wave, $-k^*i$, the moving velocity, $\text{IM}[\partial\omega^*/\partial k^*]$ and the growth rate of the amplitude of the moving wave front, $\text{RE}[\partial\omega^*/\partial k^*]$, are all positive.

3. SOLUTION METHODOLOGY AND RESULTS

Using the commercial algebra software, Mathematica 8.0 (www.wolfram.com), equation (26) is solved, subject to the following conditions for marginal convective instability: $\text{IM}[\partial\omega^*/\partial k^*] = 0$, $\text{RE}[\partial\omega^*/\partial k^*] = 0$, and $-k^*i > 0$. The values of R_c^* in the analysis varied from 1.7 to 553, the radius of the continuous liquid microtube varied from 160 to 600 μm and the ratio of the viscosities of the disperse and continuous liquids, μ_r , is taken equal unity (Table 2) for simplicity and comparison with the numerical results reported in [8]. However, in the comparisons of the results of the present analysis with the reported experimental results, the viscosity ratio is not unity and varies in values [3,6]. The analytical solution determines the values of k^* , ω^* , Ka and R_c^* , corresponding to the boundary between transition and jetting. The selected values of R_c and R_c^* in Table (2) cover a wide range of possibilities including those used in the numerical analysis reported in reference [8]

Table 2. Properties and parameters used in the present linear instability analysis.

Parameter	Value / Range	Units
Inner microtube radius, R_d	50	μm
Outer microtube radius, R_c	160 – 600	μm
Disperse liquid viscosity, μ_d	0.06	Pa·s
Continuous liquid viscosity, μ_c	0.06	Pa·s
Disperse/ continuous liquid density, ρ_d/ρ_c	1000/1000	kg/m^3
Interfacial tension, $\sigma_{d,c}$	0.02	N/m
Dimensionless outer microtube radius, $R_c^* = R_c r_j^0$	1.75 – 553	–
Microtubes' radii ratio, R^*	3.2 – 10.2	–

To express the instability analysis results in terms of the dimensionless quantities, Ca_d and $\mu_r \bar{u}_r$, the injection velocities of the disperse and continuous liquid had to be calculated. The obtained value of Ka is used to calculate the interface velocity of the basic disperse liquid flow, $u_{z,\text{int}}^0$. This interface velocity and the calculated value of R_c^* from the solution of equation (26) are used to calculate the injection flow rates of the co-flowing liquids (Q_d^0 and Q_c^0), as:

$$Q_c^0 = 0.5 u_{z,\text{int}}^0 \pi \left(\frac{R_c}{R_c^*} \right)^2 (R_c^{*2} - 1) \tag{27a}$$

and,

$$R_c^{*2} = 1 + (Q_c^0/Q_d^0) \left(1 + (1 + \mu_r (Q_d^0/Q_c^0))^{0.5} \right). \quad (27b)$$

Equation (27a) expresses the injection rate of the continuous liquid, Q_c^* , in terms of its injection velocity, $\mu_{z, \text{int}}^0$ and the radii ratio of the continuous liquid microtube and the disperse liquid jet R_c^* . Equation (27b) expresses R_c^* in terms of the injection rates and viscosity ratio of the continuous and disperse liquids. The procedures for deriving Equations (27a) and (27b) are detailed in Appendix-B.

This section presents the obtained results of the performed linear instability analysis to predict the boundary between transition and jetting for co-flowing immiscible liquids in co-axial microtube for the parameters listed in Table 1. The analysis parametrically varies the injection rates of the liquids and the radii of the coaxial microtubes. The results are validated by comparing them to those of the linear instability analysis of Herrada, G.-Calvo and Guillot [6] for aqueous solutions of glycerine and silicone oil flow in coaxial microtube with $R^* = 13.8$.

The present results are also compared to the reported experimental data by Utada et al. [3] for ionized water and PDMS (Polydimethylsiloxane) oil with $R^* = 10$. In addition, the results of the present linear instability analysis for the range of parameters in Table 2 are formulated in terms of the dimensionless quantities: Ca_d and $\mu_r \bar{u}_r$. The obtained values for the boundary between transition and jetting are compared with the results of the numerical simulations and the dimensionless correlation developed recently by the authors [8].

Figure 4 plots the injection rate of the continuous liquid versus that of the disperse liquid. It compares the present results of linear instability analysis of the boundary between transition and jetting with those reported by Herrada et al. [6], using an identical approach. The results for the conditions listed in the figure are for an aqueous solution of glycerine, as the continuous liquid, and silicon oil, as the disperse liquid. Thus, it is not surprising that the present analysis results and those of Herrada et al. [6] are identical. Nonetheless, such an agreement validates the absence of errors in the present linear instability analysis, which used to perform a parametric analysis using the liquid properties and parameters in Tables 2. The

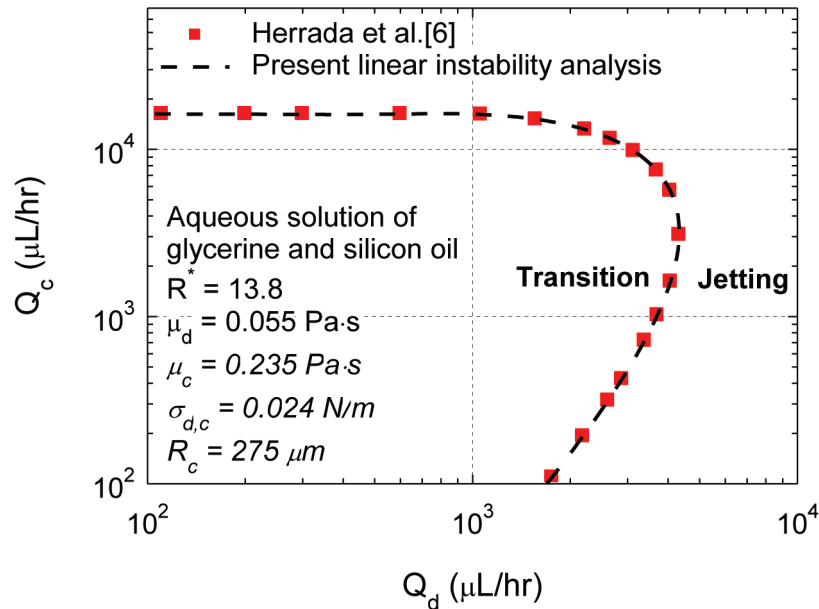


Figure 4. Comparisons of present instability analysis results with those of Herrada et al. [6].

results of this analysis are formulated in terms of the dimensionless capillary number of disperse liquid, Ca_d , and the ratio of the dynamic forces of the continuous and disperse liquids, $\mu_r \bar{u}_r$. These dimensionless quantities have been used successfully to compose flow regimes map and accurately characterize the conditions for the boundaries between dripping, transition and jetting [8]. The developed dimensionless correlation for the boundary between transition and jetting was expressed, as [8]:

$$Ca_{d,TJ} = 0.014 R^{*1.75} \left(1 + 0.01 (R^{*2} \mu_r \bar{u}_r)^{2.7} \right)^{-0.27} \tag{28}$$

In this correlation, the capillary number of the disperse liquid along that boundary between transition and jetting, $Ca_{d,TJ}$, strongly depends on the ratio of the microtubes radii, R^* , and is inversely proportional to the ratio of the dynamics forces for the co-flowing liquids, $\mu_r \bar{u}_r$. The first term on the right hand side of equation (28), $(0.014 R^{*1.75})$, is the highest Ca_d beyond which the boundary between the transition and jetting regimes becomes independent of $\mu_r \bar{u}_r$ (Figs. 5 and 6).

The developed dimensionless correlation for the boundary between dripping and transition in Figure 5 was given as [8]:

$$Ca_{d,DT} = 0.14 \left(1 + 4.63 \mu_r \bar{u}_r^{1.74} \right)^{-0.58} \tag{29}$$

In this correlation, the capillary number of the disperse liquid along that boundary, $Ca_{d,DT}$, is independent of the ratio of the microtubes radii, R^* , and solely depends on the ratio of the dynamics forces for the co-flowing liquids, $\mu_r \bar{u}_r$.

The dimensionless correlations given by equations (28) and (29) are in good agreement with the numerical simulation results of Yang and El-Genk [8], covering wide ranges of parameters and liquids

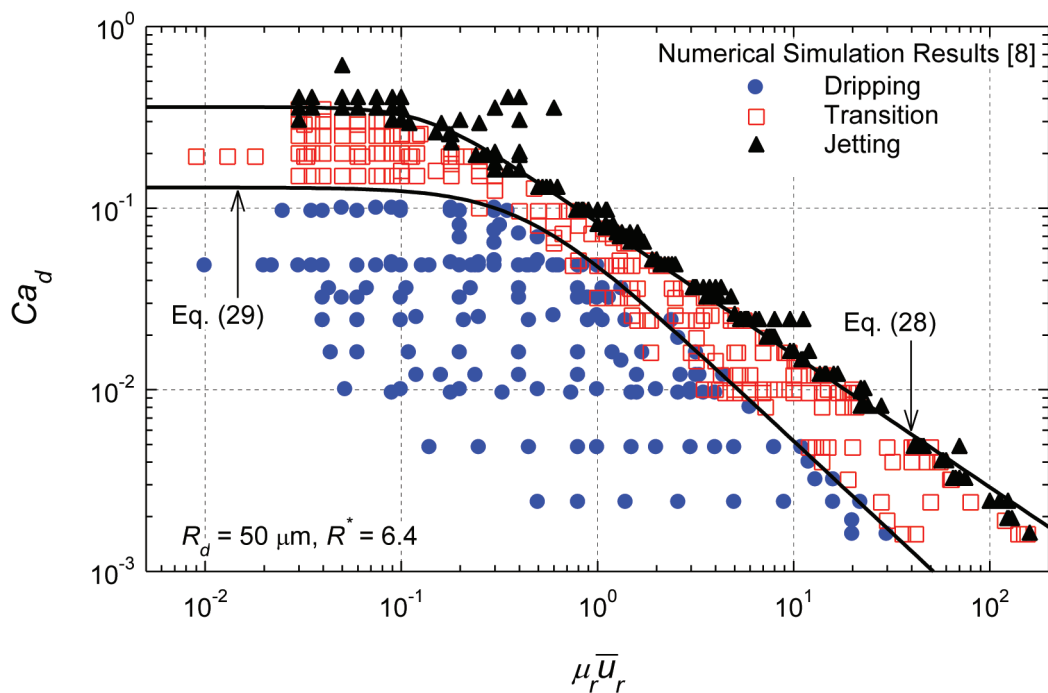


Figure 5. A flow regimes map for disperse droplets (dripping, transition and jetting).

properties. The results of the simulation were in good agreement, to within $\pm 20\%$, with the reported experimental measurements for different immiscible liquids. These include ionized water and PDMS (Polydimethylsiloxane) oil with $R^* = 10$, and aqueous solutions of glycerine into silicone oil flow with and without surfactant (Sodium Dodecyl Sulfate) with $R^* = 13.8$ [3,5,6]. The agreement validated the numerical results and confirmed the fidelity of the developed flow regimes map (Fig. 5) and of the developed semi-empirical dimensionless correlations (Equations (28) and (29)) for predicting the boundaries between dripping, transition and jetting regimes [8].

Figures 6a - 6c compare the results of the present linear instability analysis with the flow regimes map developed recently by the authors [8]. The flow regimes map in Figure 6a, for $R_d = 50$ and $100 \mu\text{m}$ and $R^* = 3.2$, incorporates a total of 147 data points, including 51 data points in the dripping regime, 36 in the transition regime and 60 in the jetting regime. The flow regimes map in Figure 6b, for $R_d = 50$ and $100 \mu\text{m}$ and $R^* = 6.4$, includes 166 data points in the dripping regime, 242 in the transition regime and 188 in the jetting regime. Figure 6c, for $R_d = 50$ and $100 \mu\text{m}$ and $R^* = 10.2$, includes 69 data points in the dripping regime, 140 in the transition regime and 53 in the jetting regime. Figures 6a - 6c also compare the present results of the linear instability analysis for $R^* = 3.2, 6.4, 10.2$ with the developed dimensionless correlation in equation (28) for the boundary between transition and jetting [8].

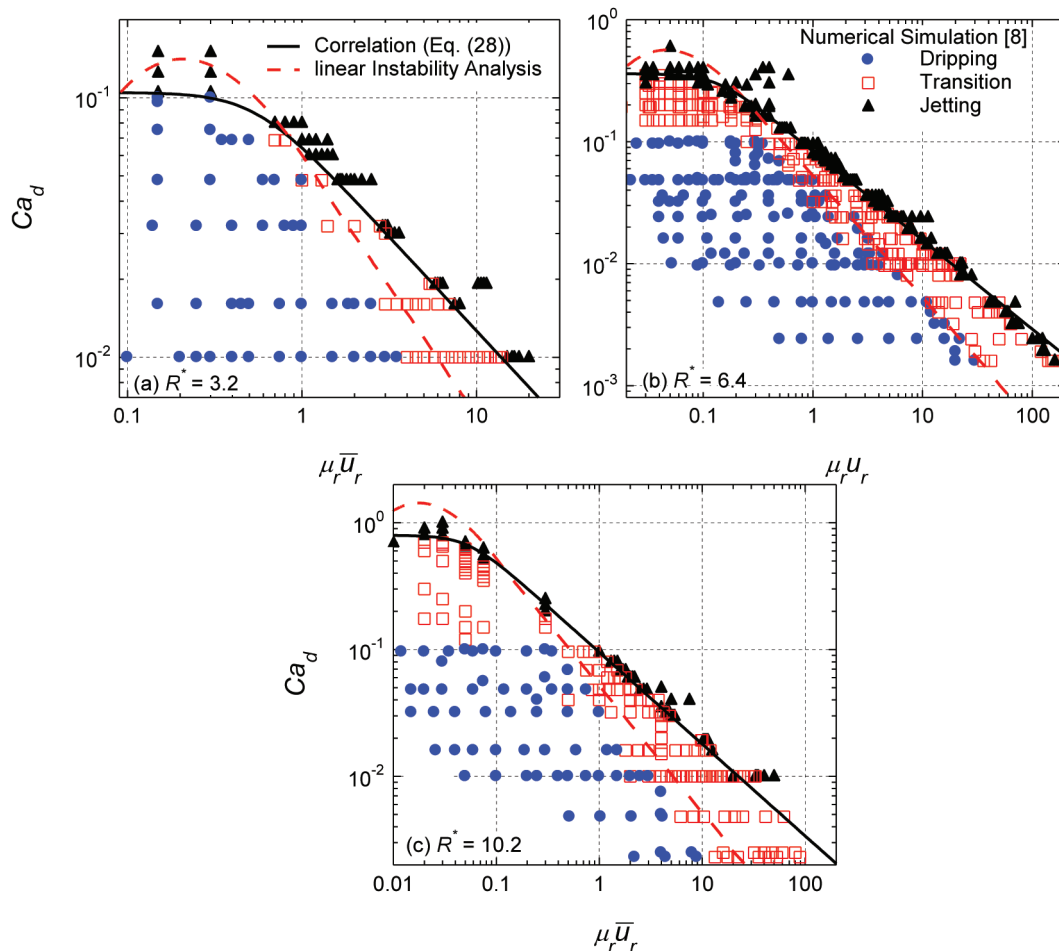


Figure 6. Comparison of present linear instability analysis results with the dimensionless correlation and numerical simulation results [8] for the boundary between transition and jetting. (a) $R^* = 3.2$, (b) $R^* = 6.4$ and (c) $R^* = 10$.

The linear instability analysis predictions of the boundary between transition and jetting are consistently lower than equation (28) at low and intermediate Ca_d values, but higher at higher Ca_d (Figures 6a-6c). At low dynamic force ratios, $\mu_r \bar{u}_r < 0.85$, the predictions of the linear instability analysis are higher than both the correlation (equation (28)) of the boundary between transition and jetting and the numerical results [8] (Fig. 6a). The difference becomes progressively smaller as $\mu_r \bar{u}_r$ increases beyond 0.85. Increasing R^* from 3.2 to 6.4 and 10.2 decreases the value of $\mu_r \bar{u}_r$ beyond which the linear instability analysis under predicts the boundary between transition and jetting. This value is $\mu_r \bar{u}_r \approx 0.4$ and 0.15 when $R^* = 6.4$ and 10.4 , respectively (Figs. 6b and 6c).

Underestimating the boundary between transition and jetting by the linear instability analysis could be attributed to neglecting higher order terms in the linearized continuity and momentum balance equations and other assumptions indicated earlier. These assumptions simplified the governing equations for obtaining a closed form analytical solution, requiring relatively much shorter time to perform the calculations than the numerical simulations [8]. Note that for low $\mu_r \bar{u}_r$, the linear instability analysis missed the trend of the boundary between transition and jetting, indicating that the corresponding Ca_d is almost independent of $\mu_r \bar{u}_r$ (Figs. 6a -6b).

In short, the under prediction of the linear stability analysis at the low values of Ca_d is mainly caused by neglecting the effect of the secondary perturbations. However, at high value of the Ca_d , the over prediction of the linear stability analysis could be attributed to neglecting not only the secondary perturbation but also the inertia of the disperse liquid.

Neglecting the secondary perturbations of the interface (Fig. 3) decreases the effective surface area of the disperse liquid jet, overestimating the total hydrodynamic energy per unit surface area corresponding to the boundary between transition and jetting. This causes the linear instability analysis predictions of the boundary between transition and jetting to occur at lower dynamic force ratios, $\mu_r \bar{u}_r$, compared to the numerical results and equation (28) [8]. The effect of neglecting the secondary perturbations of the interface in the linear instability analysis, decreases as the capillary number of

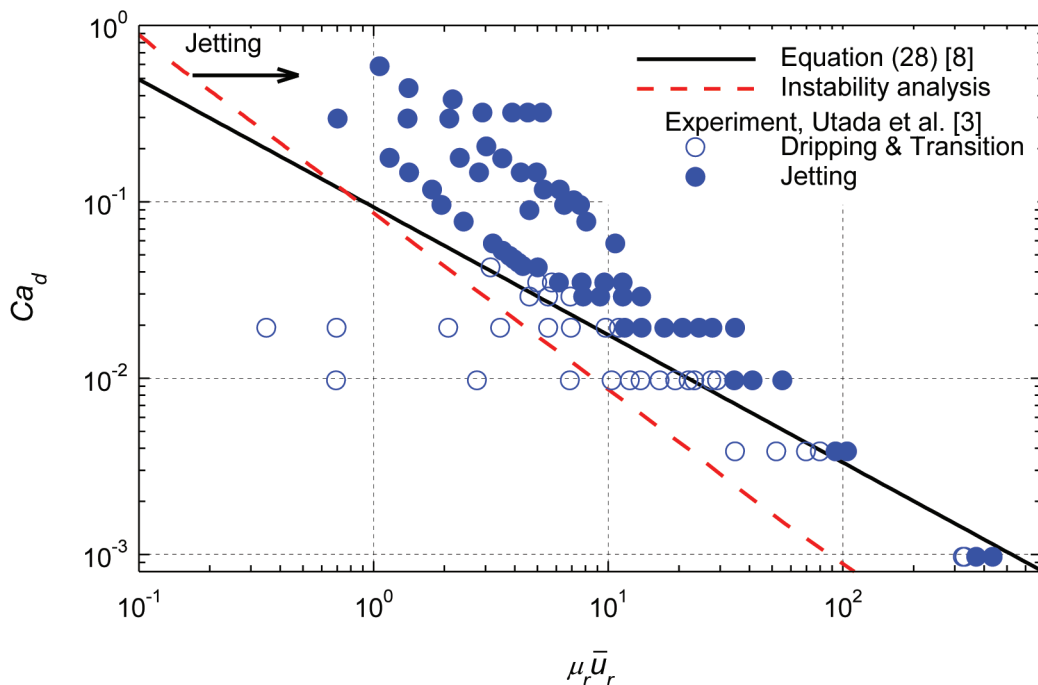


Figure 7. Comparison of the results of linear instability analysis with the experimental data of Utada et al. [3],

disperse liquid, Ca_d . The calculated values of the dynamic force ratios for the boundary between transition and jetting by the linear instability analysis gradually approach the numerical results [8], with increasing Ca_d . The difference diminishes when $Ca_d = 0.064, 0.25$, and 0.5 in Figures 6a, 6b, and 6c, respectively.

Figure 7 compares the present results of the linear instability analysis and the predictions of the correlation given in Eq. (28) with the experimental results of Utada et al. [3] for co-flowing ionized water and PDMS (Polydimethylsiloxane) oil in coaxial microtubes with $R^* = 10$. They only identified two regimes in the experiments, jetting and dripping, considering the transition regime a part of the dripping regime. The correlation in equation (28) for the boundary between transition and jetting is in good agreement with the experimental results of Utada et al. [3]. However, the linear instability analysis under predicts that boundary at low values of Ca_d , because of neglecting the secondary perturbations.

At low Ca_d , the inertia of the disperse liquid is low and its effect is negligibly small. Conversely, the linear instability analysis over predicts the boundary between jetting and transient at high Ca_d values. This is because of neglecting both the secondary perturbation and the inertia of the disperse liquid in the analysis in order to simplify the governing equations for obtaining a closed form solution, as detailed in this paper. Thus, future instability analysis needs to include both the secondary perturbations and the inertia of the disperse liquid in order to improve the solution fidelity and accuracy.

4. SUMMARY AND CONCLUSION

Results show that the linear instability analysis is an effective approach for predicting a nearly accurate boundary between the transition and jetting regimes for forming disperse droplets using co-flowing immiscible liquid in coaxial microtubes. This predicative approach is much faster than performing Computation Fluid Dynamic (CFD) simulations or conducting experiments. The analysis results, assuming disperse liquids creep flows and neglecting secondary perturbations, are identical to those of Herrada, G.-Calvo, and Guillot [6]. The analysis results are compared to a semi-empirical dimensionless correlation and flow regimes map, recently developed based on numerical simulations covering wide ranges of parameters and liquids properties [8]. They are also compared to reported experimental data by Utada et al. [3] for co-flowing ionized water and PDMS oil in coaxial microtubes.

Although captures the general trend, the linear instability analysis consistently under predicts and over predict the boundary between transition and jetting regimes at low and high Ca_d values, respectively. The difference between the linear instability analysis predictions and both the numerical simulations and the experimental results decrease as the capillary number of the disperse liquid, Ca_d , increases, or the ratio of dynamic forces for the co-flowing liquids, $\mu_r \bar{u}_r$ decreases.

At high values of Ca_d , the boundary between transition and jetting is independent of $\mu_r \bar{u}_r$. The linear instability analysis does not capture that trend. This could be attributed to the simplifying assumptions incorporated in the analysis in order to obtain a closed form analytical solution of the constituent equations and the dispersion relation, including neglecting the higher order terms for the perturbed interface and the inertia the disperse liquid. At low Ca_d , the inertia of the disperse liquid is very low and its effect is negligibly small, but neglecting the secondary perturbations causes the linear instability analysis to under predict the experimental results for the boundary between jetting and transition. Conversely, at high Ca_d values, neglecting both the secondary perturbation and the inertia of disperse liquid causes the linear instability analysis to over predict the boundary between jetting and transient. Thus, future instability analysis needs to include both the secondary perturbation and the inertia of the disperse liquid in order to improve the solution fidelity and accuracy.

NOMENCLATURE

Ca_d	Capillary number of disperse liquid, $\mu_d \bar{u}_d / \sigma_{d,c}$
$Ca_{d,DT}$	Capillary number for dripping-transition boundary.
$Ca_{d,TJ}$	Capillary number for transition- jetting boundary.
IM	Imaginary part of complex number
RE	Real part of complex number

Ka	Capillary number of basic disperse liquid flow, $\mu_d u_{z,int}^0 / \sigma_{d,c}$
k	Wave number (m^{-1})
k^*	Dimensionless wave number, $r_j^0 k$
p	Pressure (Pa)
p'	Perturbed pressure (Pa)
\bar{p}	Linearized perturbed pressure (Pa)
p^*	Dimensionless linearized perturbed pressure, $\bar{p} / (\rho_d u_{z,int}^0)^2$
Q	Liquid flow rate ($\mu l/s$)
R	Microtube radius (μm)
R^*	Microtubes radii ratio, R_c / R_d
R_c^*	Dimensionless outer microtube radius, R_c / r_j^0
Re_{int}	Reynolds number of disperse liquid at interface, $r_j^0 \rho_d u_{z,int}^0 / \mu_d$
r	Radial distance (μm)
r_j	Radius of disperse liquid jet (μm)
r^*	Dimensionless radial distance, r / r_j^0
u	Flow velocity (m/s)
u^*	Dimensionless perturbed flow velocity, u' / \bar{u}_d
u'	Perturbed flow velocity (m/s)
\hat{u}	Linearized perturbed flow velocity (m/s)
\hat{u}^*	Dimensionless linearized perturbed flow velocity $\hat{u} / \hat{u}_{z,int}^0$
\bar{u}	Average inlet flow velocity (m/s)
\bar{u}_r	Inlet flow velocity ratio, \bar{u}_c / \bar{u}_d
t	Time (s)
t^*	dimensionless time, $\hat{u}_{z,int}^0 t / r_j^0$
z	Axial distance (μm)
z^*	Dimensionless axial distance, z / r_j^0

Greek

μ	Liquid viscosity (Pa·s)
μ^*	Dimensionless Viscosity, μ / μ_d
μ_r	Viscosity ratio, μ_c / μ_d
ξ	Amplitude of interface perturbation (μm)
ξ^*	Dimensionless amplitude of interface initial wave, $\mu_d^* \Big _{r=r_j^0} / (i(\omega^* - k^*))$
ρ	Liquid density (kg/m^3)
ρ^*	Density ratio, ρ_c / ρ_d
$\sigma_{d,c}$	Interfacial tension, (N/m)
τ'	Shear tensor
ψ	Perturbed stream-function
ω	Wave frequency (1/s)
ω^*	Dimensionless wave frequency, $r_j^0 \omega / u_{z,int}^0$

Superscript

0 Basic flow

Subscript

c Continuous

d	Disperse
int	Disperse-continuous liquids interface
n	Liquid Identifier, (c = continuous or d = disperse)
r	Radial
z	Axial

ACKNOWLEDGMENTS

The University of New Mexico's Institute for Space and Nuclear Power Studies funded this research.

REFERENCES

- [1] Yang, I. H., and El-Genk, M. S., Emulsion Formation in Dripping Regime of Co-flowing Immiscible Liquids in Co-axial Micro-tubes, *Micro-Nano Scale Transport*, 2011, 2(1), 57 -83.
- [2] Cramer, C., Fischer, P., and Windhab, E. J., Drop Formation in a Co-flowing Ambient Fluid, *Chem. Eng. Sci.*, 2004, 59(15), 3045-3058.
- [3] Utada, A. S., Fernandez-Nieves, A., Stone, H. A., and Weitz, D. A., Dripping to Jetting Transitions in Coflowing Liquid Streams, *Phys. Rev. Lett*, 2007, 99(9), paper no. 094502.
- [4] Castro-Hernandez, E., Gundabala, V., Fernandez-Nieves, A., and Gordillo, J. M., Scaling the Drop Size in Coflow Experiments, *New J. Phys.*, 2009, 11(7), paper no. 075021.
- [5] Guillot, P., Colin, A., Utada, A. S., and Ajdari, A., Stability of a Jet in Confined Pressure-driven Biphase Flows at Low Reynolds Numbers, *Phys. Rev. Lett.*, 2007, 99(10), paper no. 104502.
- [6] Herrada, M. A., G.-Calvo, A. M., and Guillot, P., Spatiotemporal instability of a confined capillary jet, *Phys. Rev. E*, 2008, 78, paper no. 046312.
- [7] Colin, T., and Tancogne, S., Stability of Bifluid Jets in Microchannels, *Eur. J. Mech. B-Fluids*, 2011, 30,409-420.
- [8] Yang, I. H., and El-Genk, M. S., Numerical Analysis of co-flowing liquids in co-axial microtube: flow regimes map and correlations, *Micro-Nano Scale Transport*, 2012, 3(3&4), 79 - 102.
- [9] Rayleigh, L., On the Instability of Jets, *Proc. London Math. Soc.*, 1879, 10, 4-13.
- [10] Rayleigh, L., On the Instability of a Cylinder of Viscous Liquid under Capillary Force, *Phil. Mag.*, 1892,34, 145-154.
- [11] Tomotika, S., On the Instability of a Cylindrical Thread of a Viscous Liquid Surrounded by Another Viscous Fluid, *Proc. R. Soc. Lond. A*, 1935, 150(870), 322-327.
- [12] Keller, J. B., Rubinow, S. I., and Tu, Y. O., 1973, "Spatial instability of a jet," *Phys. Fluids*, 16(12), pp. 2052-2055.
- [13] Leib, S. J., and Goldstein, M. E., The Generation of Capillary Instabilities on a Liquid Jet, *J. Fluid. Mech.*, 1986, 168, 479-500.
- [14] Leib, S. J., and Goldstein, M. E., Convective and Absolute Instability of a Viscous Liquid Jet, *Phys. Fluids*, 29(4), 1986, 952-954.
- [15] Huerre, P., and Monkewitz, P. A., Local and Global Instabilities in Spatially Developing Flows, *Annu. Rev. Fluid. Mech.*, 1990, 22, 473-537.
- [16] Saarloos, W. V., Front Propagation into Unstable State: Marginal Stability as a Dynamical Mechanism for Velocity Selection, *Phys. Rev. A*, 1988, 37(1), 211-229.
- [17] Saarloos, W. V., Front Propagation into Unstable States, *Phys. Rep.*, 2003, 386, 29-229.
- [18] O'Donnel, B., Chen, J. N., and Lin, S. P., Transition from Convective to Absolute Instability in a Liquid Jet, *Phys. Fluids*, 2001, 13(9), 2732-2734.
- [19] Guillot, P., Colin, A., and Ajdari, A., Stability of a Jet in Confined Pressure-Driven Biphase Flows at Low Reynolds Number in Various Geometries, *Phys. Rev. E.*, 2008, 99(10), paper no. 016307.
- [20] Ashgriz, N, *Handbook of Atomization and Sprays*, New York, Springer, 2011.

- [21] Jog, C. S., *Foundations and Applications of Mechanics: Fluid Mechanics*, Boca Raton, CRC Press, 2002.
- [22] Gu, Y., Kojima, H., and Miki, N., Theoretical Analysis of 3D Emulsion Droplet Generation by a Device Using Coaxial Glass Tubes, *Sens. Actuators A: Phys.*, 2011, 169(2), 326-332.
- [23] Hua, J., Zhang, B., and Lou, J., Numerical Simulation of Microdroplet Formation in Coflowing Immiscible Liquids, *AIChE Journal*, 2007, 53(10), 2534-2547.

Appendix-A

This appendix presents the functions DN and NM used in equation (26) for calculating the determinant of the square matrix (equation (24)). These functions are fully expanded in terms of Ka , R_c^* and μ_r in equations (A.1) and (A.2) below:

$$\begin{aligned}
 DN = & (1/k^*) ((\mu_r - 1)^2 k^{*3} (R_c^* k^*) K_0(R_c^* k^*) + K_1(R_c^* k^*) (2 K_0(R_c^* k^*) - R_c^* k^* K_1(R_c^* k^*))) I_0(k^*)^4 + \\
 & (\mu_r - 1)^2 k^{*2} (R_c^* k^* ((k^* - \mu_r k^*) K_0(k^*) + \mu_r K_1(k^*)) I_0(R_c^* k^*)^2 + (-2(\mu_r - 1) R_c^* k^* I_1(k^*) K_0(R_c^* k^*) - \\
 & (\mu_r - 1) k^* K_0(k^*) (R_c^* k^* K_0(R_c^* k^*) + 2 K_1(R_c^* k^*)) + K_1(k^*) ((\mu_r - 1) I_1(R_c^* k^*) k^{*2} - (\mu_r - 2) R_c^* K_0(R_c^* \\
 & k^*) k^* + ((\mu_r - 1) (R_c^{*2} + 1) k^{*2} + 2 \mu_r) K_1(R_c^* k^*))) + I_0(R_c^* k^*) + 2(\mu_r - 1) I_1(k^*) K_1(R_c^* k^*) (R_c^* k^* K_1(R_c^* \\
 & k^*) - 2 K_0(R_c^* k^*)) + I_1(R_c^* k^*) + (K_1(k^*) ((\mu_r - 1) R_c^{*2} k^{*2} (2(\mu_r - 2) K_0(R_c^* k^*) + R_c^* k^* K_1(R_c^* k^*)) - 2(\mu_r \\
 & - 1) k^* K_0(k^*) (R_c^* k^* K_1(R_c^* k^*) - K_0(R_c^* k^*))) I_0(k^*)^3 + k^* (-R_c^* k^* (-\mu_r - 1)^2 k^{*2} K_0(k^*)^2 + 2(\mu_r - 1) k^* \\
 & K_1(k^*) K_0(k^*) + ((\mu_r - 1)^2 k^{*2} + (\mu_r - 2) \mu_r) K_1(k^*)^2 + (\mu_r - 1) I_1(k^*) ((2 - 3\mu_r) k^* K_0(k^*) + ((\mu_r - 1) k^{*2} + \\
 & 3\mu_r) K_1(k^*))) I_0(R_c^* k^*)^2 + (-\mu_r - 1)^2 R_c^* k^* (2k^{*2} + 1) K_0(R_c^* k^*) I_1(k^*)^2 + (\mu_r - 1) (I_1(R_c^* k^*) ((\mu_r - 1) k^* \\
 & K_0(k^*) - 2\mu_r K_1(k^*)) k^{*2} + K_0(k^*) (\mu_r R_c^* k^* K_0(R_c^* k^*) + ((\mu_r - 1) (R_c^{*2} + 1) k^{*2} + 6\mu_r - 4) K_1(R_c^* k^*))) \\
 & k^* K_1(k^*) (R_c^* k^* (\mu_r - (\mu_r - 1) k^{*2}) K_0(R_c^* k^*) - 2((\mu_r (R_c^{*2} + 1) - 1) k^{*2} + 3\mu_r) K_1(R_c^* k^*))) I_1(k^*) + 2 I_1 \\
 & (R_c^* k^*) (-\mu_r - 1)^2 k^{*2} K_0(k^*)^2 + 2(\mu_r - 1) k^* K_1(k^*) K_0(k^*) + ((\mu_r - 1)^2 k^{*2} + (\mu_r - 2) \mu_r) K_1(k^*)^2)) I_0(R_c^* \\
 & k^*) + R_c^* k^* I_1(R_c^* k^*)^2 (-\mu_r - 1)^2 k^{*2} K_0(k^*)^2 + 2(\mu_r - 1) k^* K_1(k^*) K_0(k^*) + ((\mu_r - 1)^2 k^{*2} + (\mu_r - 2) \mu_r) \\
 & K_1(k^*)^2 + (\mu_r - 1)^2 (2k^{*2} + 1) I_1(k^*)^2 K_1(R_c^* k^*) (R_c^* k^* K_1(R_c^* k^*) - 2K_0(R_c^* k^*)) + (\mu_r - 1) I_1(k^*) \\
 & I_1(R_c^* k^*) (k^* K_0(k^*) ((\mu_r - 1) R_c^{*2} k^{*2} - 2\mu_r) K_0(R_c^* k^*) + 2(2\mu_r - 1) R_c^* k^* K_1(R_c^* k^*)) - 2 K_1(k^*) ((\mu_r \\
 & (R_c^{*2} - 1) + 1) k^{*2} + \mu_r) K_0(R_c^* k^*) + R_c^* k^* ((\mu_r - 1) k^{*2} + \mu_r) K_1(R_c^* k^*))) I_0(k^*)^2 + I_1(k^*) (R_c^* k^* ((\mu_r - 1) \\
 & I_1(k^*) (k^* ((\mu_r - 1) k^{*2} - 2\mu_r - 1) K_0(k^*) + \mu_r (k^{*2} + 2) K_1(k^*)) + 2\mu_r (-\mu_r - 1) k^{*2} K_0(k^*)^2 + k^* K_1(k^*) K_0(k^*) \\
 & + (\mu_r - 1) (k^{*2} + 1) K_1(k^*)^2)) I_0(R_c^* k^*)^2 - (-2(\mu_r - 1)^2 R_c^* k^* (k^{*2} + 1) K_0(R_c^* k^*) I_1(k^*)^2 + (\mu_r - 1) (I_1 \\
 & (R_c^* k^*) (2\mu_r k^* K_0(k^*) + ((\mu_r - 1) k^{*2} - 1) K_1(k^*)) k^{*2} + K_0(k^*) (R_c^* k^* ((1 - \mu_r) k^{*2} - 2\mu_r + 1) K_0(R_c^* k^*) \\
 & + 2((\mu_r R_c^{*2} + 1) k^{*2} + 2\mu_r + 1) K_1(R_c^* k^*)) k^* + K_1(k^*) (R_c^* k^* ((2 - 3\mu_r) k^{*2} - 2\mu_r + 2) K_0(R_c^* k^*) + ((\mu_r \\
 & - 1) (R_c^{*2} + 1) k^{*4} - (R_c^{*2} + 2\mu_r + 1) k^{*2} - 4\mu_r) K_1(R_c^* k^*))) I_1(k^*) + 4\mu_r I_1(R_c^* k^*) (-\mu_r - 1) k^{*2} K_0(k^*)^2 \\
 & + k^* K_1(k^*) K_0(k^*) + (\mu_r - 1) (k^{*2} + 1) K_1(k^*)^2) I_0(R_c^* k^*) + 2\mu_r R_c^* k^* I_1(R_c^* k^*)^2 ((\mu_r - 1) k^{*2} K_0(k^*)^2 - \\
 & k^* K_1(k^*) K_0(k^*) - (\mu_r - 1) (k^{*2} + 1) K_1(k^*)^2 - 2(\mu_r - 1)^2 (k^{*2} + 1) I_1(k^*)^2 K_1(R_c^* k^*) R_c^* k^* K_1(R_c^* k^*) - \\
 & 2K_0(R_c^* k^*)) + (\mu_r - 1) I_1(k^*) I_1(R_c^* k^*) (K_1(k^*) ((-\mu_r - 1) R_c^{*2} k^{*4} + (R_c^{*2} - 6\mu_r + 4) k^{*2} - 4\mu_r + 4) \\
 & 2K_0(R_c^* k^*) + 2(2\mu_r - 1) R_c^* k^* (k^{*2} + 1) K_1(R_c^* k^*)) + 2k^{*2} K_0(k^*) ((-\mu_r R_c^{*2} - \mu_r + 1) K_0(R_c^* k^*)) + R_c^* \\
 & k^* ((\mu_r - 1) k^{*2} - 1) K_1(R_c^* k^*))) I_0(k^*) + I_1(k^*)^2 (R_c^* k^* ((-\mu_r - 1)^2 k^{*3} + 2\mu_r k^* - k^*) K_0(k^*)^2 + 2(\mu_r - 1) (\\
 & k^{*2} + 1) K_1(k^*) K_0(k^*) + (\mu_r - 1)^2 k^* (k^{*2} + 1) K_1(k^*)^2 - (\mu_r - 1) I_1(k^*) ((\mu_r - 2) k^* - 2) K_0(k^*) - (\mu_r - 1) \\
 & k^* (k^{*2} + 1) K_1(k^*))) I_0(R_c^* k^*)^2 + ((\mu_r - 1)^2 R_c^* k^* (k^{*2} + 1) K_0(R_c^* k^*) I_1(k^*)^2 - (\mu_r - 1) (((\mu_r - 1) k^{*2} - 1) \\
 & I_1(R_c^* k^*) K_0(k^*) k^{*2} - (\mu_r - 1) (k^{*2} + 1) K_1(k^*) (R_c^* k^* K_0(R_c^* k^*) + 2K_1(R_c^* k^*)) k^* + K_0(k^*) ((\mu_r - 1) \\
 & (R_c^{*2} + 1) k^{*4} - (R_c^{*2} - 2\mu_r + 5) k^{*2} - 4) K_1(R_c^* k^*) - \mu_r R_c^* k^* K_0(R_c^* k^*))) I_1(k^*) + 2 I_1(R_c^* k^*) (((\mu_r - 1) \\
 & 1)^2 k^{*3} - 2\mu_r k^* + k^*) K_1(k^*)^2 - 2(\mu_r - 1) (k^{*2} + 1) K_1(k^*) K_0(k^*) - (\mu_r - 1)^2 k^* (k^{*2} + 1) K_1(k^*)^2)) I_0(R_c^* k^*) \\
 & - k^* ((\mu_r - 1)^2 (k^{*2} + 1) K_1(R_c^* k^*) (R_c^* k^* K_1(R_c^* k^*) - 2K_0(R_c^* k^*) I_1(k^*)^2 - (\mu_r - 1) I_1(R_c^* k^*) (K_0(k^*) \\
 & (k^* ((\mu_r - 1) k^{*2} - 1) k^{*2} - 1) R_c^{*2} + 2\mu_r) 2K_0(R_c^* k^*) - 2 R_c^* (k^{*2} + 1) K_1(R_c^* k^*)) - 2(\mu_r - 1) (k^{*2} + 1) \\
 & K_1(k^*) (R_c^* k^* K_1(R_c^* k^*) - K_0(R_c^* k^*))) I_1(k^*) + R_c^* I_1(R_c^* k^*)^2 ((-\mu_r - 1)^2 k^{*3} + 2\mu_r k^* - k^*) K_0(k^*)^2 + \\
 & 2(\mu_r - 1) (k^{*2} + 1) K_1(k^*) K_0(k^*) + (\mu_r - 1)^2 k^* (k^{*2} + 1) K_0(k^*)^2))). \tag{A.1}
 \end{aligned}$$

$$\begin{aligned}
 NM = & (\mu_r k^{*2} I_0(R_c^* k^*) K_I(k^*) (I_I(R_c^* k^*) + K_I(R_c^* k^*)) I_0(k^*)^3 + k^* (\mu_r R_c^* k^* K_I(k^*) (I_I(k^*) + K_I(k^*)) \\
 & I_0(R_c^* k^*)^2 + (-\mu_r - 1) R_c^* k^* K_0(R_c^* k^*) I_0(k^*)^2 + \mu_r (I_I(R_c^* k^*) (k^* K_0(k^*) 2K_I(k^*)) - R_c^* k^* K_0(R_c^* k^*) \\
 & K_I(k^*) + (k^* K_0(k^*) - 4K_I(k^*)) K_I(R_c^* k^*)) I_I(k^*) + 2\mu_r I_I(R_c^* k^*) K_I(k^*)^2 I_0(R_c^* k^*) + \mu_r R_c^* k^* I_I(R_c^* \\
 & k^*)^2 + 2\mu_r I_I(k^*) I_I(R_c^* k^*) K_I(k^*) (K_0(R_c^* k^*) - R_c^* k^* K_I(R_c^* k^*)) + (\mu_r - 1) I_I(k^*)^2 K_I(R_c^* k^*) (R_c^* k^* \\
 & K_I(R_c^* k^*) - 2K_0(R_c^* k^*))) I_0(k^*)^2 + I_I(k^*) (R_c^* k^* (2\mu_r K_I(k^*)^2 + I_I(k^*) (2\mu_r K_I(k^*) - k^* K_0(k^*))) I_0(R_c^* \\
 & k^*)^2 - (-2(\mu_r - 1) R_c^* k^* K_0(R_c^* k^*) I_I(k^*)^2 + k^* I_I(R_c^* k^*) (2\mu_r K_0(k^*) + (\mu_r - 1) k^* K_I(k^*)) + k^* K_0(k^*) \\
 & (R_c^* k^* K_0(R_c^* k^*) + 2(\mu_r + 1) K_I(R_c^* k^*)) - K_I(k^*) (2(\mu_r - 1) R_c^* k^* K_0(R_c^* k^*) + ((R_c^* k^* - \mu_r + 1) k^{*2} + \\
 & 4\mu_r) K_I(R_c^* k^*))) I_I(k^*) + 4\mu_r I_I(R_c^* k^*) K_I(k^*)^2 I_0(R_c^* k^*) - 2\mu_r R_c^* k^* I_I(R_c^* k^*)^2 K_I(k^*)^2 - 2(\mu_r + 1) \\
 & I_I(k^*)^2 K_I(R_c^* k^*) (R_c^* k^* K_I(R_c^* k^*) - 2K_0(R_c^* k^*)) + I_I(k^*) I_I(R_c^* k^*) (2k^* K_0(k^*) (K_0(R_c^* k^*) - R_c^* k^* \\
 & K_I(R_c^* k^*)) + K_I(k^*) ((R_c^* k^* K_I(R_c^* k^*) - 2K_0(R_c^* k^*)) + 2(2\mu_r + 1) R_c^* k^* K_I(R_c^* k^*))) I_0(k^*) + I_I(k^*)^2 (R_c^* \\
 & k^* (k^* K_0(k^*)^2 + 2K_I(k^*) K_0(k^*) + (\mu_r - 1) k^* K_I(k^*)^2 + I_I(k^*) (2K_0(k^*) + (\mu_r - 1) k^* K_I(k^*))) I_0(R_c^* k^*)^2 + \\
 & ((\mu_r - 1) R_c^* k^* K_0(R_c^* k^*) I_I(k^*)^2 + (-\mu_r - 1) I_I(R_c^* k^*) K_0(k^*) k^2 + (\mu_r - 1) R_c^* K_0(R_c^* k^*) K_I(k^*) k^2 + \\
 & (((R_c^* k^* - \mu_r + 1) k^{*2} + 4) K_0(k^*) + 2(\mu_r - 1) k^* K_I(k^*)) K_I(R_c^* k^*)) I_I(k^*) - 2I_I(R_c^* k^*) (k^* K_0(k^*)^2 + \\
 & 2K_I(k^*) K_0(k^*) + (\mu_r - 1) k^* K_I(k^*)^2) I_0(R_c^* k^*) + k^* ((\mu_r - 1) K_I(R_c^* k^*) (2K_0(R_c^* k^*) - R_c^* k^* K_I(R_c^* k^*)) \\
 & I_I(k^*)^2 + I_I(R_c^* k^*) R_c^* K_0(k^*) (R_c^* k^* K_0(R_c^* k^*) + 2K_I(R_c^* k^*)) - 2(\mu_r - 1) K_I(k^*) (K_0(R_c^* k^*) - R_c^* k^* \\
 & K_I(R_c^* k^*))) I_I(k^*) - R_c^* I_I(R_c^* k^*)^2 (k^* K_0(k^*)^2 + 2K_I(k^*) K_0(k^*) + (\mu_r - 1) k^* K_I(k^*)^2))). \quad (A.2)
 \end{aligned}$$

Appendix-B

This appendix presents the derivations of Equations (27a) and (27b) in section 3 on the solution methodology and results in the main text. For steady state and unperturbed interface, the momentum balance equation is expressed as:

$$0 = -\nabla P_n^0 + \mu_n \nabla^2 u_{z,n}^0 \tag{B.1}$$

The velocity fields for the continuous and disperse liquids can be obtained from the solution of Equation (B.1) based on the following conditions: (a) non-slip at the wall of the outer tube of the

continuous liquid $(u_{z,c}^0|_{r^*=R_c^*} = 0)$, (b) continuity of the velocity and shear stress at the interface $(u_{z,c}^0|_{r^*=1} = u_{z,d}^0|_{r^*=1} \text{ and } \mu_d \frac{\partial u_{z,d}^0}{\partial r}|_{r^*=1} = \mu_c \frac{\partial u_{z,c}^0}{\partial r}|_{r^*=1})$, and (c) no perturbations of the interface $(u_{r,c}^0 = 0 \text{ and } u_{r,d}^0 = 0)$. The solution gives for the following velocity fields:

$$u_{z,c}^0 = -\frac{\nabla P^0}{4\mu_c} (R_c^{*2} - r^{*2}), \quad \text{for } (1 \leq r^* \leq R_c^*) \tag{B.2}$$

$$u_{z,d}^0 = \frac{\nabla P^0}{4\mu_d} \left\{ r^{*2} - \frac{R_c^{*2}}{\mu_r} \left(1 + \frac{\mu_r - 1}{R_c^{*2}} \right) \right\}, \quad \text{for } (0 \leq r^* \leq 1) \tag{B.3}$$

Equations (B.2 and B.3) are expressed in a dimensionless form by dividing by the flow velocity at the interface $(u_{z,int}^0 = \frac{\nabla P^0}{4\mu_c} (R_c^{*2} - 1))$, which gives:

$$U_{z,c}^0 = 1 + \frac{1 - r^{*2}}{R_c^{*2} - 1} \tag{B.4a}$$

$$U_{z,d}^0 = 1 + \mu_r \frac{1 - r^{*2}}{R_c^{*2} - 1} \tag{B.4b}$$

The injection flow rates of the continuous and disperse liquids are determined from integrating the fully-developed flow velocities over the cross-section flow area, as:

$$Q_n^0 = 2\pi \int r_j^{0^2} r^* u_{z,int}^0 U_{z,n}^0 dr^* \tag{B.5}$$

The result gives the following expression of the volumetric flow rate of the continuous, same as Equation (27a) in the main text, as:

$$Q_c^0 = \frac{1}{2} u_{z,\text{int}}^0 \pi \left(\frac{R_c}{R_c^*} \right)^2 (R_c^{*2} - 1) \quad (\text{B.6})$$

In addition, these dimensionless expressions are obtained:

$$Q_d^0 = \frac{1}{2} u_{z,\text{int}}^0 \pi \left(\frac{R_c}{R_c^*} \right)^2 \left(\frac{2R_c^{*2} + u_r - 2}{R_c^{*2} - 1} \right) \quad (\text{B.7a})$$

$$\frac{Q_c^0}{Q_d^0} = \frac{(R_c^{*2} - 1)^2}{2R_c^{*2} + \mu_r - 2} \quad (\text{B.7b})$$

Inverting Equation (B.7b) gives [6]:

$$R_c^{*2} = 1 + \frac{Q_c^0}{Q_d^0} \left(1 + \left(1 + \mu_r \frac{Q_d^0}{Q_c^0} \right)^{0.5} \right) \quad (\text{B.8})$$

This equation is the same as Equation (27b) in the main text.

